MECHANICAL CHARACTERIZATION OF 2-D, 2-D STITCHED, AND 3-D BRAIDED/RTM MATERIALS

Jerry W. Deaton
NASA Langley Research Center
Hampton , Virginia

Susan M. Kullerd
and
Marc A. Portanova
Lockheed Engineering and Sciences Company
Hampton, Virginia

INTRODUCTION

Braided composite materials have potential for application in aircraft structures. Fuselage frames, floor beams, wing spars, and stiffeners are examples where braided composites could find application if cost effective processing and damage tolerance requirements are met. Another important consideration for braided composites relates to their mechanical properties and how they compare to the properties of composites produced by other textile composite processes being proposed for these applications. Unfortunately, mechanical property data for braided composites do not appear extensively in the literature. Data are presented in this paper on the mechanical characterization of 2-D triaxial braid, 2-D triaxial braid plus stitching, and 3-D (through-the-thickness) braid composite materials. The braided preforms all had the same graphite tow size and same nominal braid architectures, [±30°/0°], and were resin transfer molded (RTM) using the same mold for each of two different resin systems. Static data are presented for notched and unnotched tension, notched and unnotched compression, and compression after impact strengths at room temperature. In addition, some static results, after environmental conditioning, are included.

Baseline tension and compression fatigue results are also presented, but only for the 3-D braided composite material with one of the resin systems.

Figure 1 outlines the objective and approach utilized in characterizing the braided composites reported herein. An architecture of [±30°/0°] was selected for both 2-D triaxial and 3-D braid preform fabrication and RTM to assess the potential of braided composites for aircraft structures. This architecture was selected since single pass coverage could be accomplished using a 12K graphite tow in the 2-D triaxial braid which would result in a higher volume fraction and be more cost-effective in building up panel thickness by using the larger graphite tow size. The materials selected, panel fabrication, and mechanical property characterization will be discussed in more detail.

OBJECTIVE AND APPROACH

Objective: Assess potential of (±30°/0°) braid architectures for resin transfer molded aircraft structures by mechanical property characterization

- Benefits sought from ±30°/0° configurations:
  - Single pass coverage
  - Higher fiber volume fraction
  - Potential cost saving of 12K tows

Approach: Braided material selection

- Braid architectures
- Fiber
- Resins

Fabrication of panels

Characterization of mechanical properties

- Static
- Fatigue

BRAID ARCHITECTURE

An artist's conception of the two braid architectures evaluated are shown in figure 2. The 2-D triaxial braid preforms were braided by Fiber Innovations, Inc., using two ends of Hercules AS4 graphite 12K tow in the +30° and -30° directions, two ends of Hercules AS4 graphite 12K, and one end of Hercules AS4 graphite 3K tow in the axial, or 0°, direction. The additional 3K tow was necessary for equal amounts of graphite (per inch) in each tow direction. Since stitching has been shown to improve the damage tolerance of other textile composites (ref. 1-3), the 2-D triaxial braid was also evaluated with stitching. Both stitched and unstitched 2-D preforms were resin transfer molded using either British Petroleum E905L resin or Ciba Geigy XUMY722/RD91-103 resin. Hereafter, the British Petroleum and Ciba Geigy resins are referred to as E905L and MY722, respectively. The 3-D braid preforms were braided by Atlantic Research Company using one end of Hercules AS4 graphite 12K tow in each of the +30°, -30°, and 0° directions, resulting in equal amounts of graphite fibers in each direction, as was the case for the 2-D triaxial braids. The 3-D braid preforms were braided in a single pass, then resin transfer molded only with E905L resin. All resin transfer molding was performed by Fiber Innovations, Inc. None of the 3-D braided preforms were stitched. Additional fabrication and processing parameters will be given subsequently.

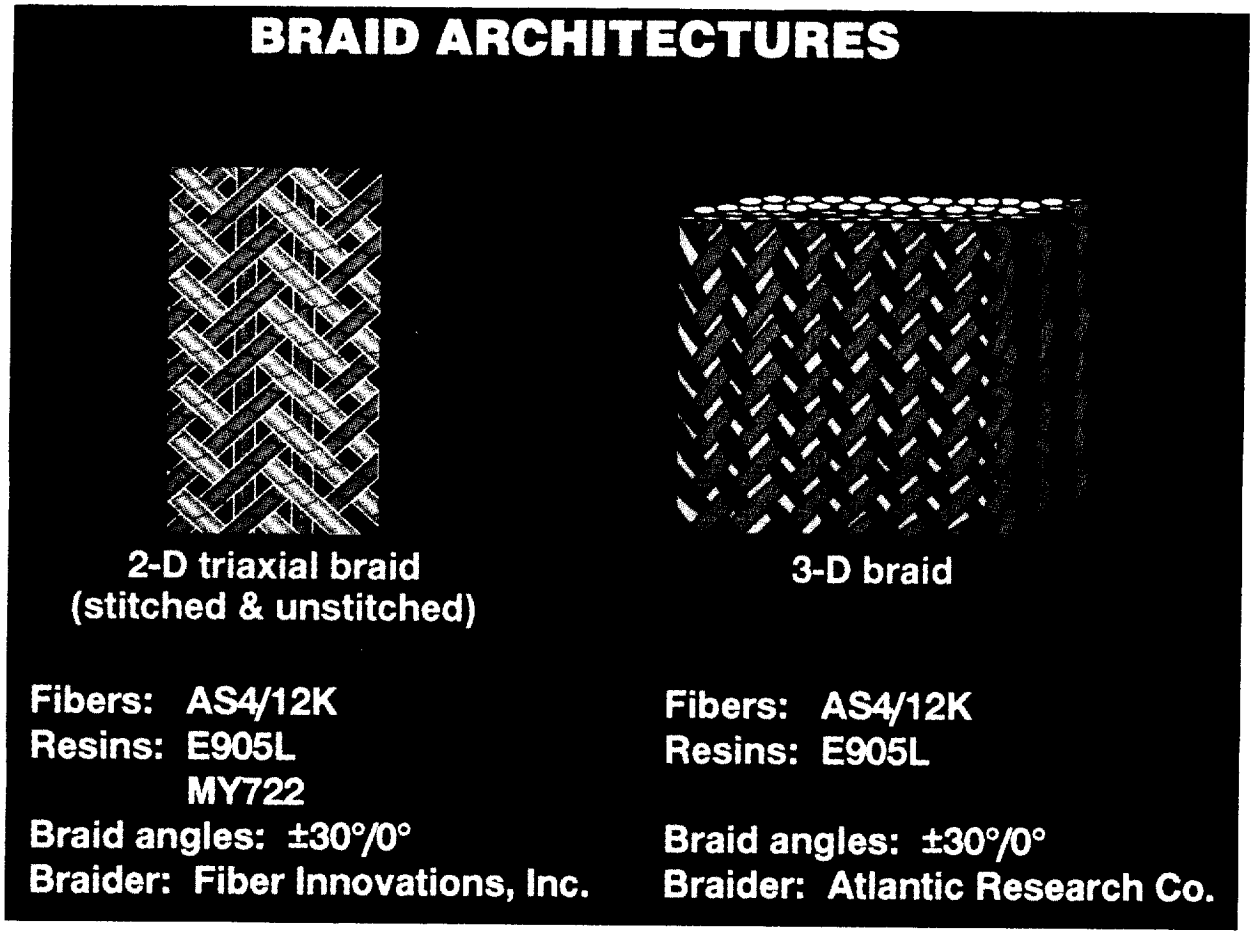

FABRICATION OF PANELS

Figure 3 outlines the fabrication procedure for 2-D and 3-D braided composites. The 2-D triaxial braid preforms were braided as cylinders using multiple passes to obtain either 3 or 6 layers, then slit along the cylinder generator. The cut edges were then stitched to maintain the braid angles. The braided cylinder length and diameter were selected such that the flat preforms would be approximately 7 inches wide and 20 inches long. Half of the 2-D braided laminates were stitched using a lock stitch and S-2 glass needle and bobbin threads. The stitch pitch was eight stitches per inch and stitch row and column spacing was nominally 0.25-inch. The 3-D braid preforms were also braided as a cylinder, but unlike the 2-D braids, the 3-D braids were braided in a single pass for each thickness. All braided preforms were RTM in the same mold for each thickness, resulting in the same nominal fiber volume fraction for each architecture and thickness. All braided laminates were nominally 0.125-inch thick for tension coupons and 0.25-inch thick for compression coupons.

FABRICATION OF PANELS

- Braid as cylinders
  - 2-D triaxial braids of 3 or 6 layers
  - 3-D braid of two thicknesses in single pass
- Slit braided preforms along cylinder generator
  - Stitch cut edges to maintain braid angle
  - Stitch one-half of 2-D triaxial preforms using 1/4 inch rows and columns
- RTM using same mold for all braid architectures
  - 0.125 in. thick for tension
  - 0.250 in. thick for compression

PHOTOMICROGRAPHS OF 2-D AND 3-D BRAIDS

Figures 4a and 4b show photomicrographs of sections indicating 0°, 90°, +30°, and -30° graphite fiber tow orientations for typical 2-D triaxial and 3-D braid architectures, respectively. The 2-D braids had an inplane nominal fiber volume fraction of 59 % and the 3-D braids had an inplane nominal fiber volume fraction of 52 %. The 0° views for the 2-D and 3-D braids appear very similar, however, the 0° graphite fiber tows shown for the 3-D braid are more evenly distributed through the thickness. Comparing the other views, respectively, indicates that the 2-D braid layers nest together with only small resin pockets whereas the 3-D braid has more and larger resin rich areas (which is consistent with the measured fiber volume fractions) with a repeating graphite tow orientation. The +30° view in figure 4b shows the graphite fiber tows traversing through the thickness, giving the composite true through-the-thickness reinforcement.

PHOTOMICROGRAPHS OF 2-D TRIAXIAL BRAID ARCHITECTURE

V_f = 59%

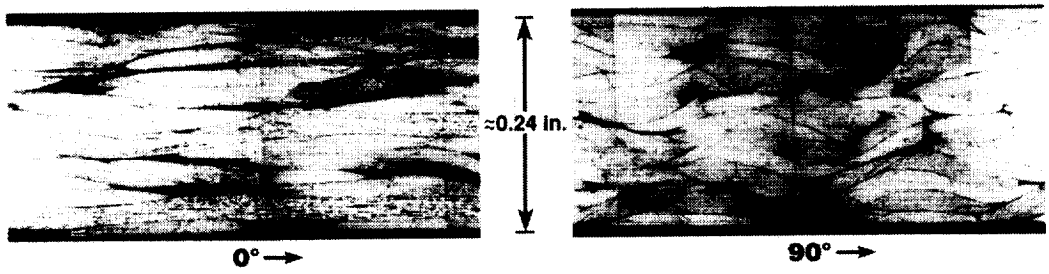

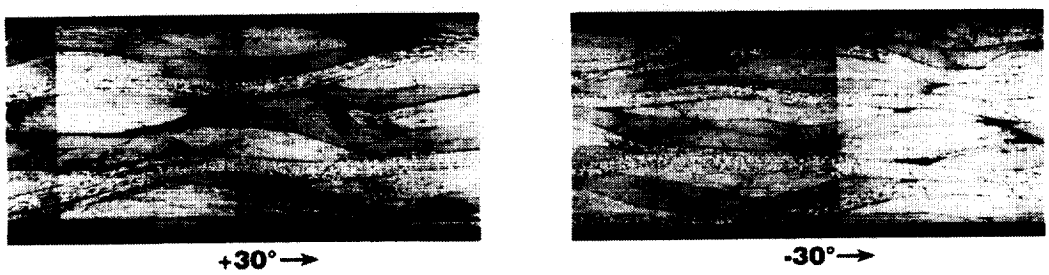

PHOTOMICROGRAPHS OF 3-D BRAID ARCHITECTURE

V_f = 52%

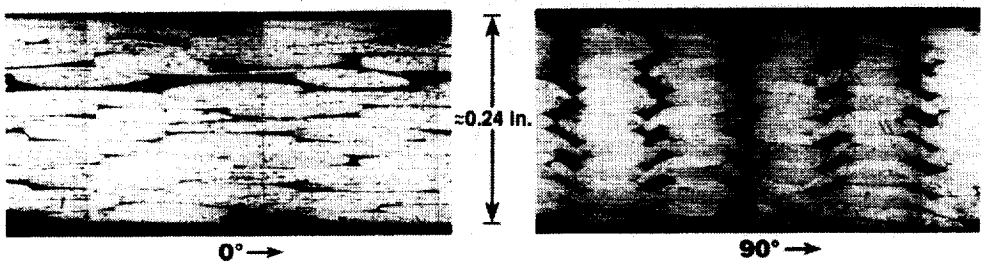

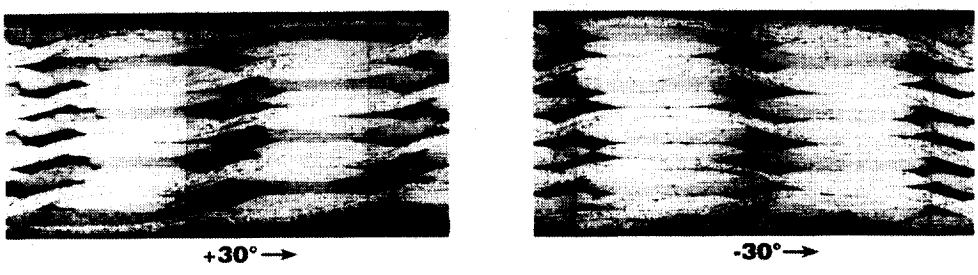

STATIC TEST SPECIMENS

The static test specimen geometries are shown in figure 5. The unnotched tension specimens were nominally 0.125-inch thick. All other specimen thicknesses were nominally 0.25-inch. Specimen lengths and widths are indicated on the figure. The short block compression specimen is a NASA Langley configuration suitable for tests of cross-plied laminates and was instrumented with 0.125-inch long stacked back-to-back strain gages. All other specimen configurations were instrumented with 0.250-inch long back-to-back axial strain gages. In addition, the unnotched tension specimens had 0.250-inch long back-to-back transverse strain gages. The compression after impact specimens were impacted at a nominal impact energy of 30 ft-lbs with the NASA Langley air gun using a 0.50-inch diameter aluminum ball as the impactor. The notched tension specimens had a 0.25-inch diameter hole. There were three notched compression specimen configurations. The 3-inch wide notched compression specimen had either a 0.25-inch or 0.50-inch diameter hole and the 5-inch wide specimen had a 1.00-inch diameter hole.

The short block compression, notched compression, and compression after impact specimens were end-clamped to prevent brooming and were tested to failure at 0.05-inch/minute in a 120-kip capacity hydraulic test machine. The open-hole compression and compression after impact fixtures also had knife-edge side supports. The tension and open-hole tension specimens were end-gripped with hydraulic grips in a 50-kip capacity servo-hydraulic test machine and were also loaded to failure at 0.050-inch/minute. Load, strain, and displacement were recorded continuously for all tests using an IBM PC-based data acquisition system.

STATIC TEST SPECIMEN CONFIGURATIONS

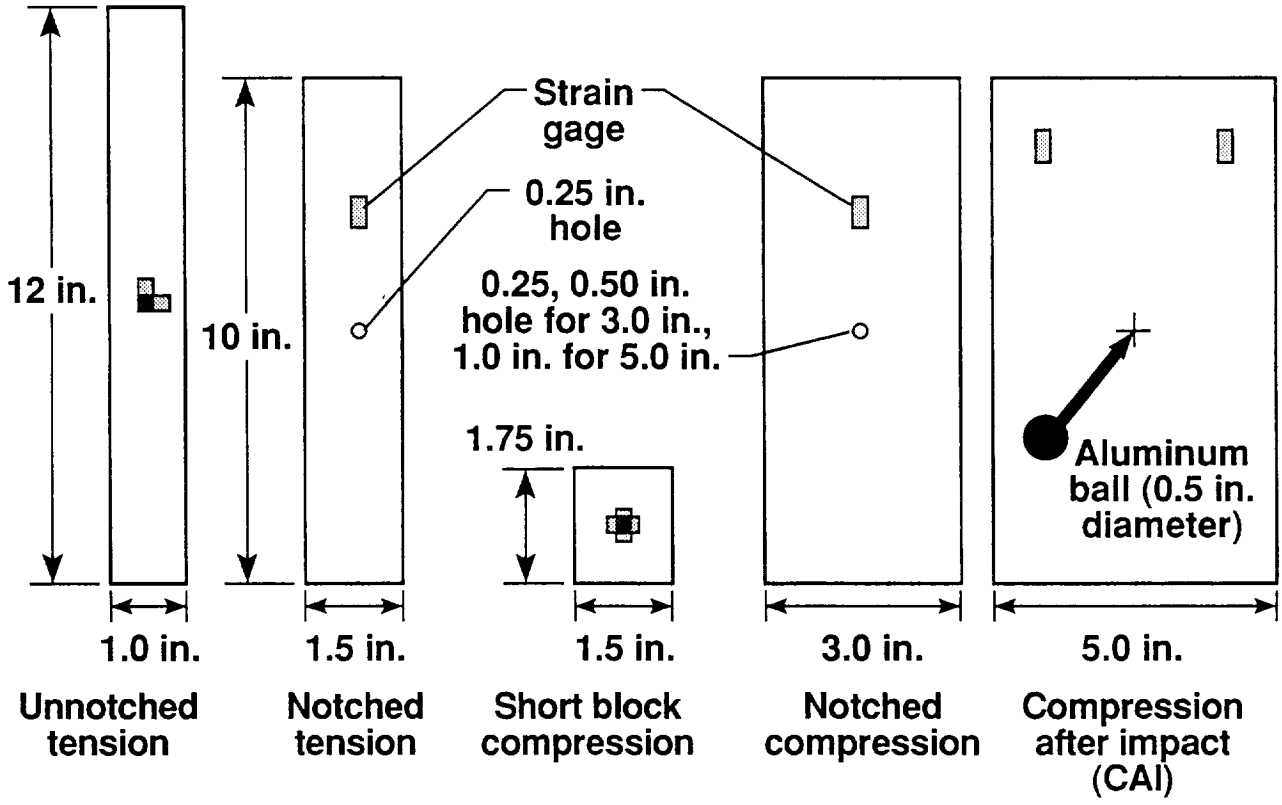

FATIGUE TEST SPECIMEN CONFIGURATIONS

Figure 6 shows the test specimen configurations for the 3-D braid material evaluated in fatigue. All specimen thicknesses were nominally 0.25-inch. Dimensions are given for both tension and compression specimens for each configuration shown in the figure. The tension specimens have longer grip lengths to allow for clamping and load transfer through shear. The compression specimens are all end loaded. Test section gage lengths were chosen to minimize buckling/instability problems in compression. The test section for both tension and compression unnotched specimens were reduced from an overall width of 1.5-in. to 1.0-in. by machining a large radius in the test section which assures that failures occur within the test section. Two notched configurations are being evaluated in fatigue. The 1.5-inch wide notched specimens have a 0.25-inch diameter hole and the 3.0-inch wide specimens have a 0.50-inch diameter hole. The 0.50-inch hole was chosen to provide access to monitor damage initiation and growth inside the hole. The compression or tension after impact specimens are being impacted using a drop-weight impactor at three different energy levels. An impact energy level of 30 ft-lbs will be evaluated first. Subsequent energy levels will depend on the results of these first tests.

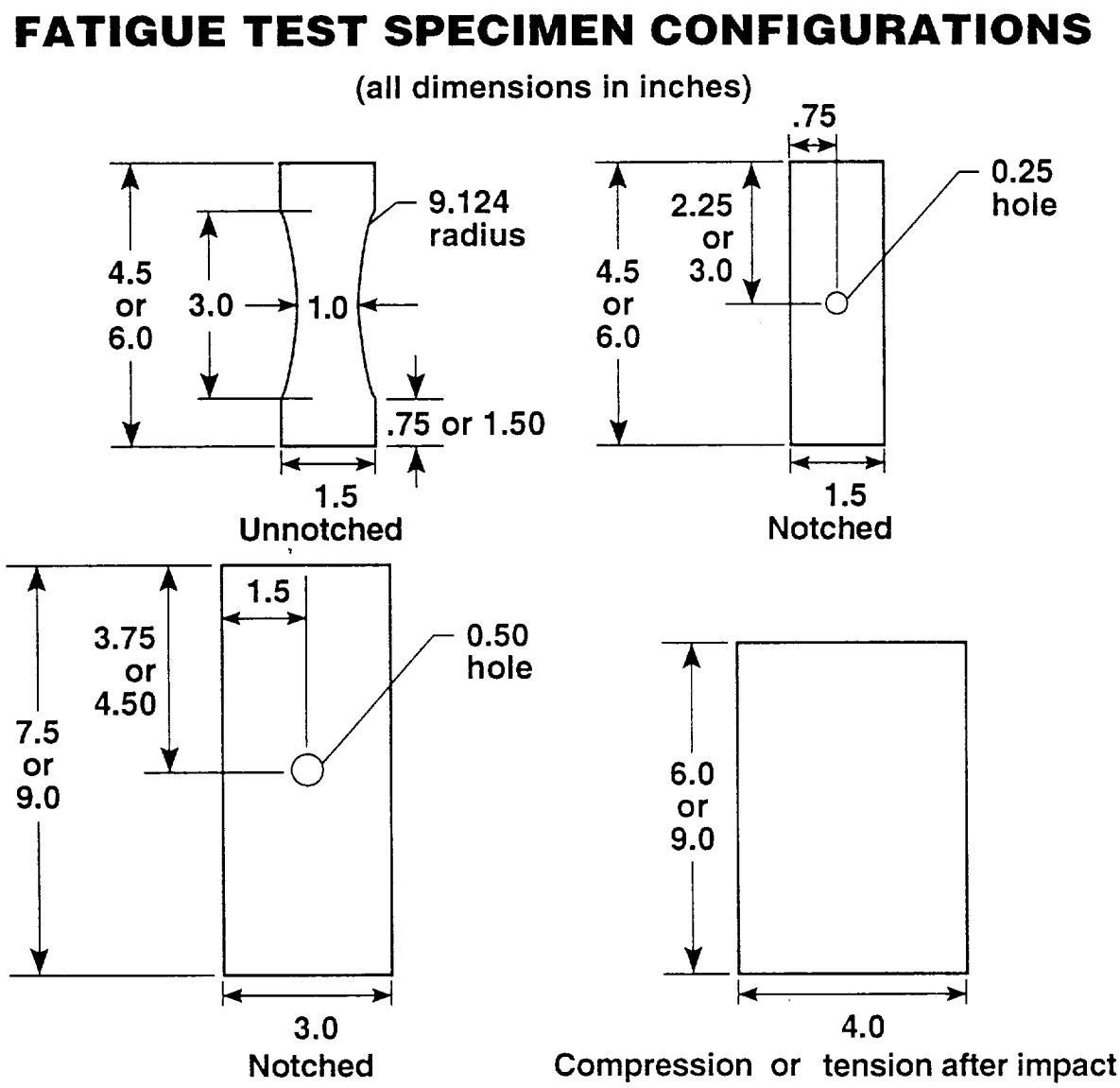

STATIC TENSILE STRENGTHS

Figure 7 shows the room temperature tensile strengths for each braid architecture and resin system evaluated in this investigation. The unshaded bars represent the average value obtained from the unnotched tests and the shaded bars are the average value obtained from the notched tests. The averages shown have not been normalized to a common fiber volume fraction. The range of values obtained from all tests is also shown on the figure. Six unnotched specimens were tested for each braid architecture and resin combination and either 2 or 3 notched specimens were tested for each combination. The tensile strength of the 3-D braid/E905L is about 6% greater than the tensile strength shown for the 2-D braid/E905L even though it has the lower fiber volume fraction. This could be attributed to the even distribution of 0° fibers through the thickness in the 3-D braid as well as the tensile contribution from the straight segments of the ±30° graphite fiber tows compared to the nested graphite tows for the 2-D braid (see fig. 4). The tensile strength of the 2-D/E905L is approximately 13% greater than that shown for 2-D/MY722. Since tension properties are fiber dominated and each 2-D braid had the same graphite fiber and braiding parameters, this difference is unexplained. Stitching resulted in about a 20% reduction in unnotched tensile strength for the 2-D braid/E905L. The notched tensile strengths exhibited only a slight reduction due to stitching. This may be due to greater stitching damage in the thinner (0.125-in.) unnotched specimens compared to the thicker (0.25-in.) notched specimens.

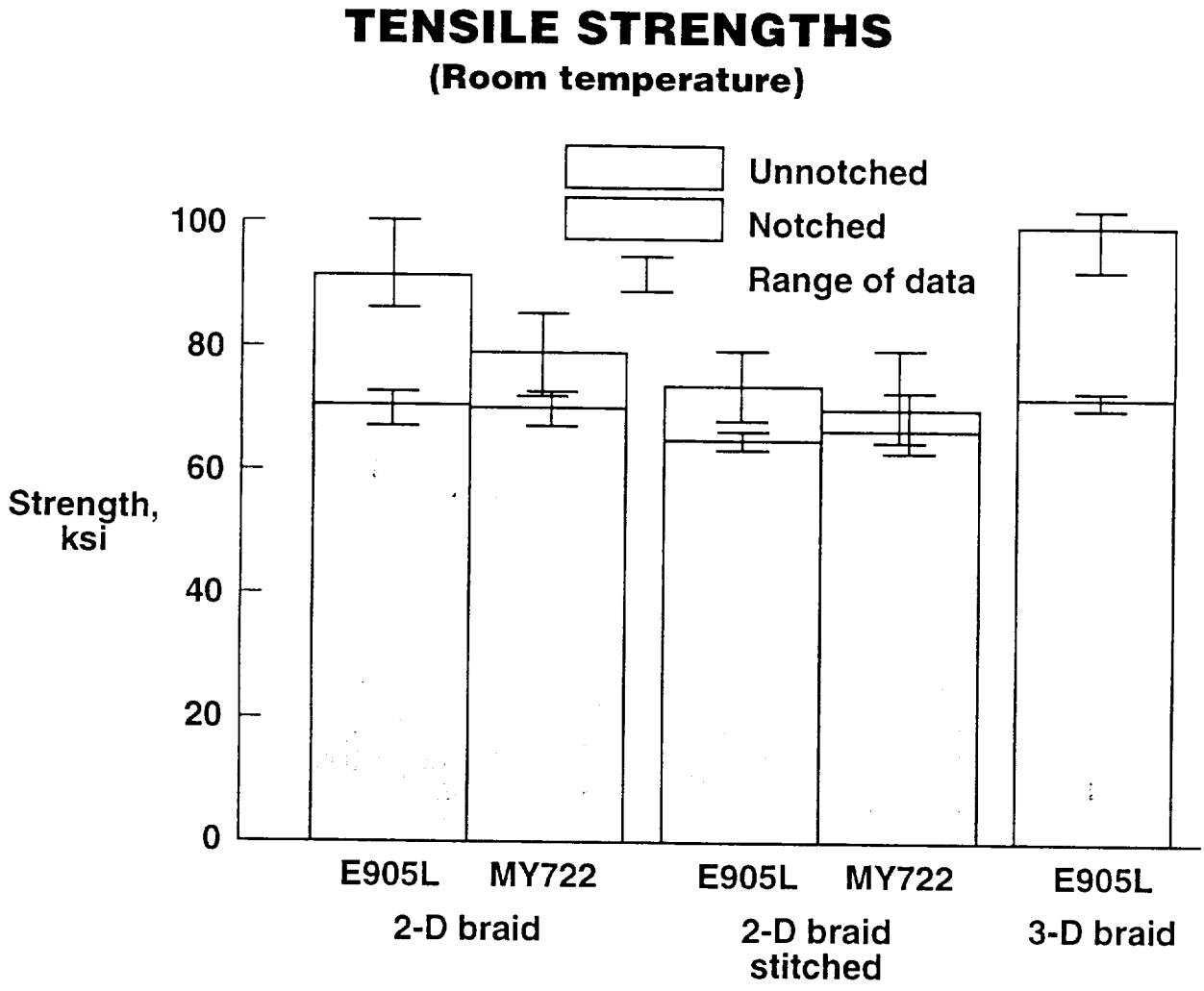

TENSILE MODULI

The average tensile modulus for each braid architecture and resin system is shown in figure 8, along with the range of values obtained. Moduli were calculated by a linear regression over the range of 0.1% to 0.3% strain to eliminate any initial loading artifacts. Also shown on the figure are tension moduli predictions for both the 2-D and 3-D braid architectures. The predicted values were obtained using a 3-D finite element analysis (ref. 4 & 5) approach to analyze a detailed unit cell of each braid architecture. Extensive use is made of photomicrographs, as shown in figure 4, to develop representative unit cell models for the finite element analysis. The measured values for the 2-D and 3-D braids are about the same whereas the 2-D braided composites with stitching are slightly less, possibly due to stitching damage to the fiber tows in the (0.125-in.) thin specimens. The 2-D prediction is shown to be excellent while the 3-D prediction is slightly less than the measured values.

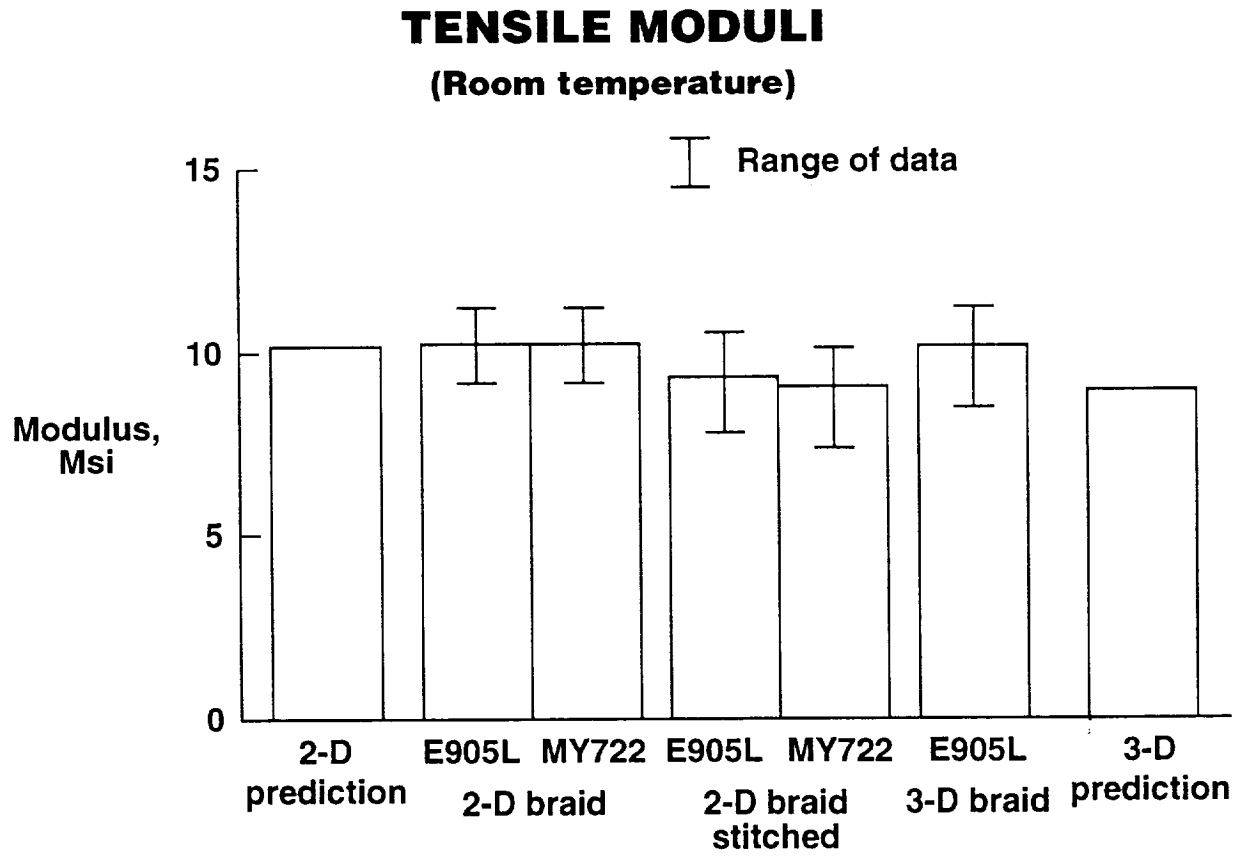

Figure 9 shows the room temperature compressive strengths for each braid and resin evaluated. The average unnotched compressive strengths were obtained from the short block compression specimens and are given by the unshaded bars. The shaded bars represent the average value obtained from the notched compression tests. Four unnotched and two notched specimens were tested for each braid architecture and resin system shown. The range of data values are also shown for each case. The 3-D braid/E905L is shown to have 10% and 15% higher unnotched compression strength than the 2-D braid/E905L and stitched 2-D braid/E905L composites, respectively. The 3-D/E905L also has the highest notched compressive strength, 15% greater than the 2-D/E905L, and 20% greater than the stitched 2-D/E905L composites. The unnotched strengths for the two stitched 2-D braid composites are the same whereas the unnotched compression strength of the 2-D braid/MY722 is considerably less than that for the 2-D braid/E905L. This is similar to the differences noted for the tensile strengths discussed in figure 7 and is also unexplained. However, one would not expect the inplane unnotched strength to increase with stitching as is indicated for the stitched 2-D braid/MY722.

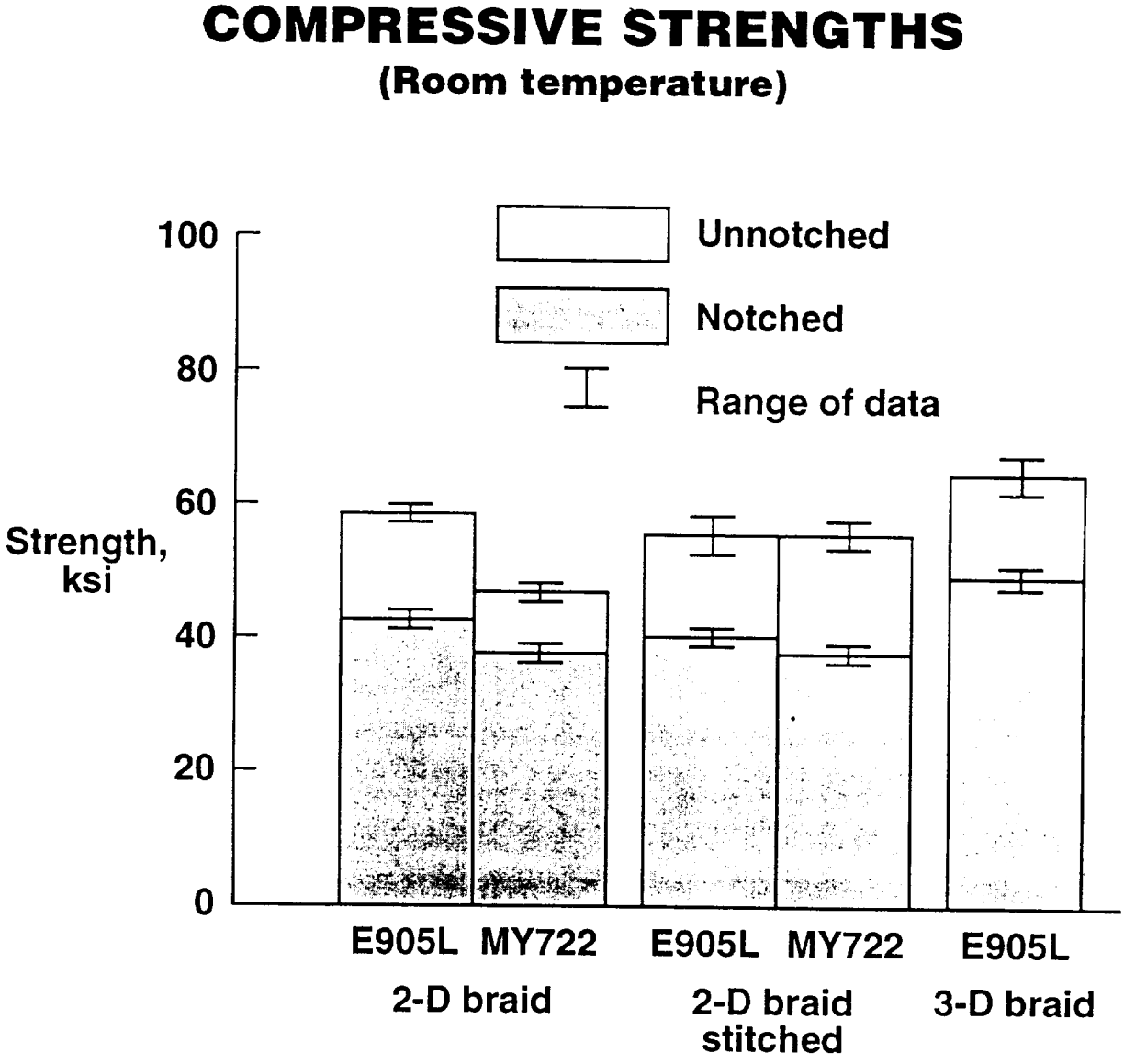

COMPRESSIVE MODULI

The average compressive modulus for each braid architecture and resin system is shown in figure 10. Compressive moduli were also calculated by a linear regression over the range of 0.1% to 0.3% strain to eliminate any initial loading artifacts. Also shown on the figure are compressive moduli predictions for the 2-D and 3-D braid architectures. The predictions were based on the 3-D finite element analysis discussed previously. The measured value for the 3-D braid is slightly less than that of the 2-D braid composites. The 2-D and 3-D predictions are shown to be slightly more than the average measured values but are within the range of measured values obtained for both braids.

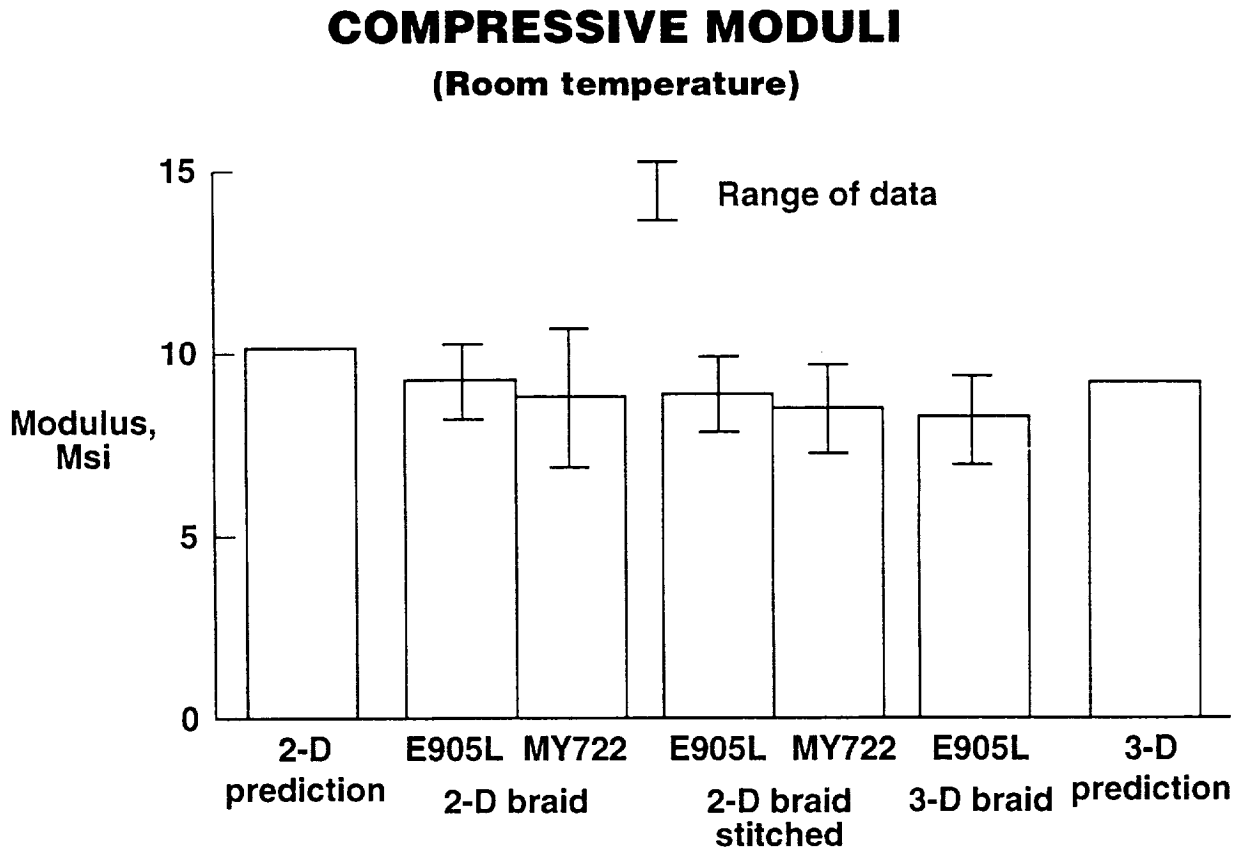

Figure 11 shows the compressive strengths for each braid architecture and resin system tested at 180° F after being soaked in 160° F water for 45 days. The average hot/wet unnotched compressive strengths were obtained from short block compression specimens and are represented on the figure by the unshaded bars. The hot/wet notched strengths are indicated by the shaded bars. Four unnotched specimens and two notched specimens were tested for each braided composite evaluated except for the notched MY722 composites where only one specimen was tested. Comparison of the hot/wet unnotched compression strengths (fig. 11) with the room temperature unnotched compression strengths (fig. 9) indicates that the 2-D/E905L and 3-D/E905L strengths are only reduced about 5% whereas the stitched 2-D/E905L strength is reduced about 17% due to the environmental conditioning and elevated temperature testing. The same trend is also noted for the notched strength comparisons (figs. 9 & 11) of the 2-D/E905L and 3-D/E905L where a reduction of about 7% was obtained for the hot/wet condition and the stitched 2-D/E905L experienced a larger reduction of about 11%. The best compression performance observed for the 3-D braids at room temperature (fig. 9) also occurs in the hot/wet test (fig. 11).

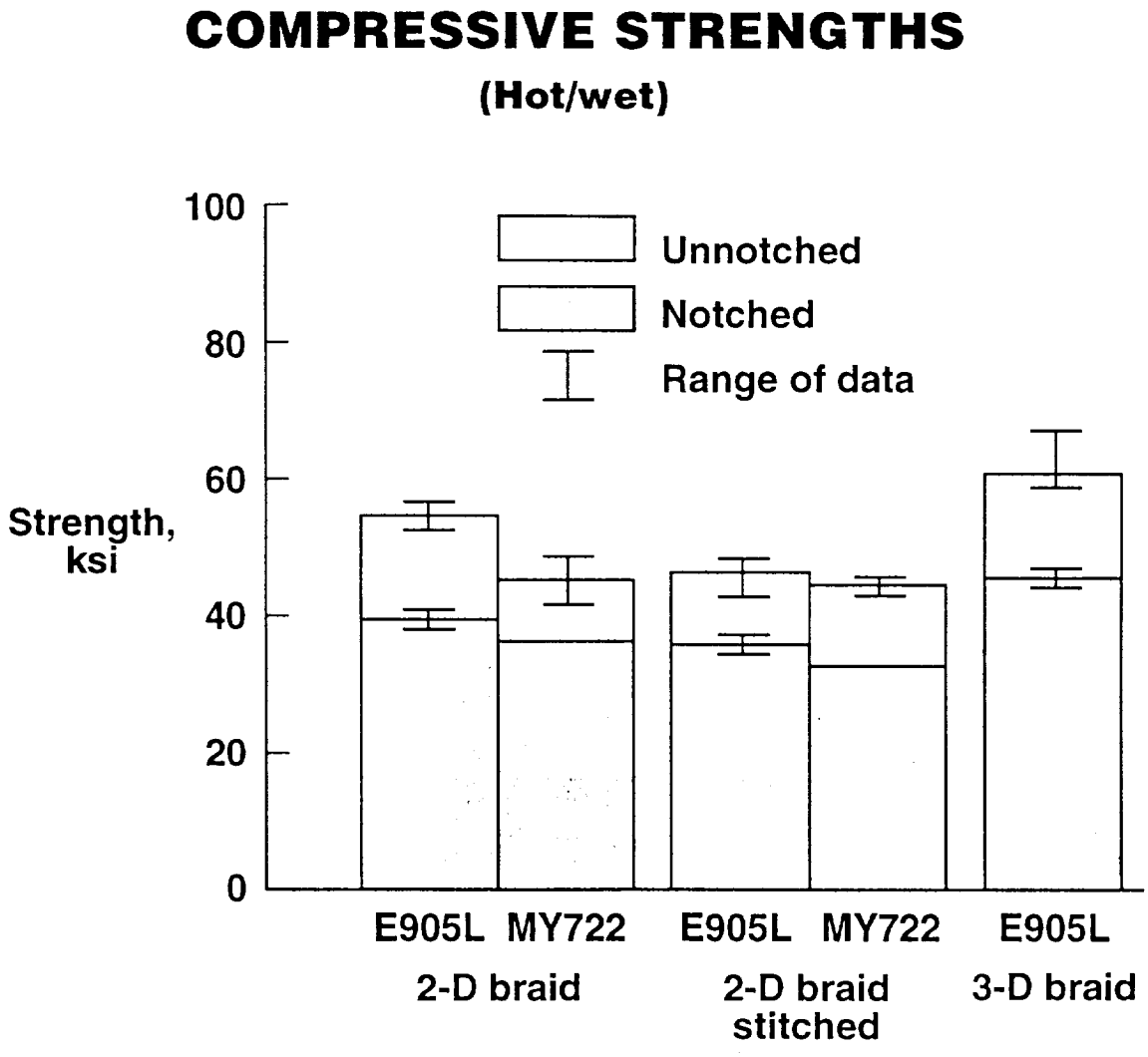

POISSON'S RATIO

Average values of Poisson's ratio obtained from both the unnotched tension and compression test for each braided composite are shown in figure 12. Also shown on the figure are the predicted values obtained from the 3-D finite element analysis discussed previously. Note that the analysis for this particular 2-D braid architecture, [±30°/0°], predicts values of Poisson's ratio greater than 1.0, which is within the range of measured values for the 2-D/E905L and 2-D/MY722 composites. The average value measured for the 3-D/E905L is almost identical to the predicted value whereas the average values measured for the 2-D/E905L and 2-D/MY722 are slightly less than the predicted value. This difference could be due to small variations in the ±30° braid angles for the 2-D braid architectures (see fig. 11 of ref. 5).

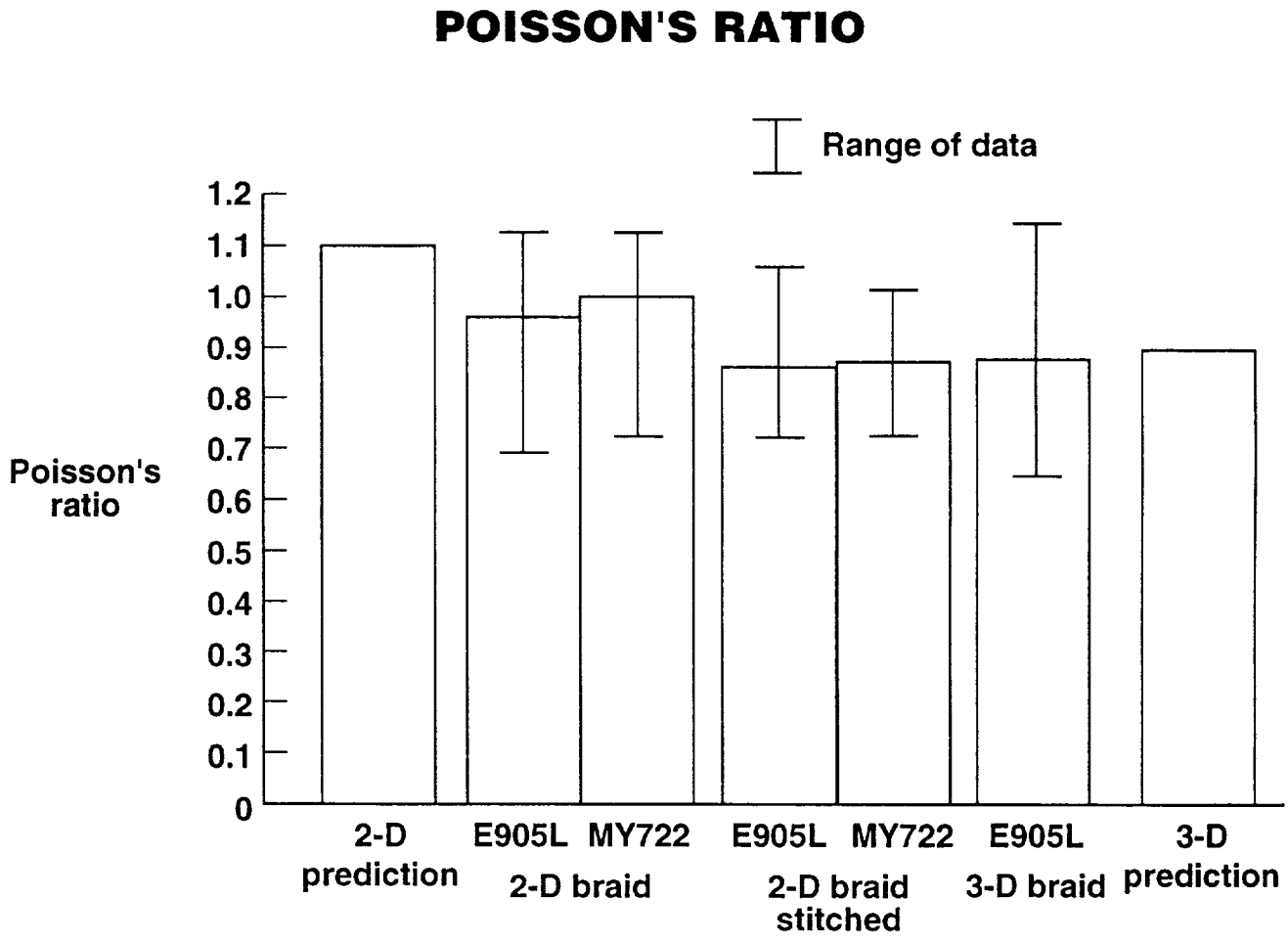

ROOM TEMPERATURE COMPRESSION AND COMPRESSION AFTER IMPACT STRENGTHS

Figure 13 shows the compression and compression after impact (CAI) strength properties measured for each braided composite under evaluation. The unshaded bars are the room temperature unnotched compression strengths from figure 9 and the shaded bars are the average room temperature CAI strengths. Three specimens were impacted for each braid and resin system (two specimens for room temperature testing and one for hot/wet testing) and the range of room temperature CAI strength values is indicated on the figure. The numbers shown in parenthesis at the top of the shaded bars represent the average damage area (2 room temperature and 1 hot/wet specimen) as determined from C-scans obtained after impact. The CAI strength of the stitched 2-D/E905L is the only braided composite which exceeded 40 ksi and is approximately 12% greater than the CAI strength of both the stitched 2-D/MY722 and 3-D/E905L composites. Comparison of the stitched 2-D braids with the unstitched 2-D braids indicates a 20% to 25% greater CAI strength increase due to stitching. This improved CAI performance is also consistent with the smaller damage areas for the respective stitched configurations. However, it should be noted that the 3-D/E905L braided composite had the smallest average damage area.

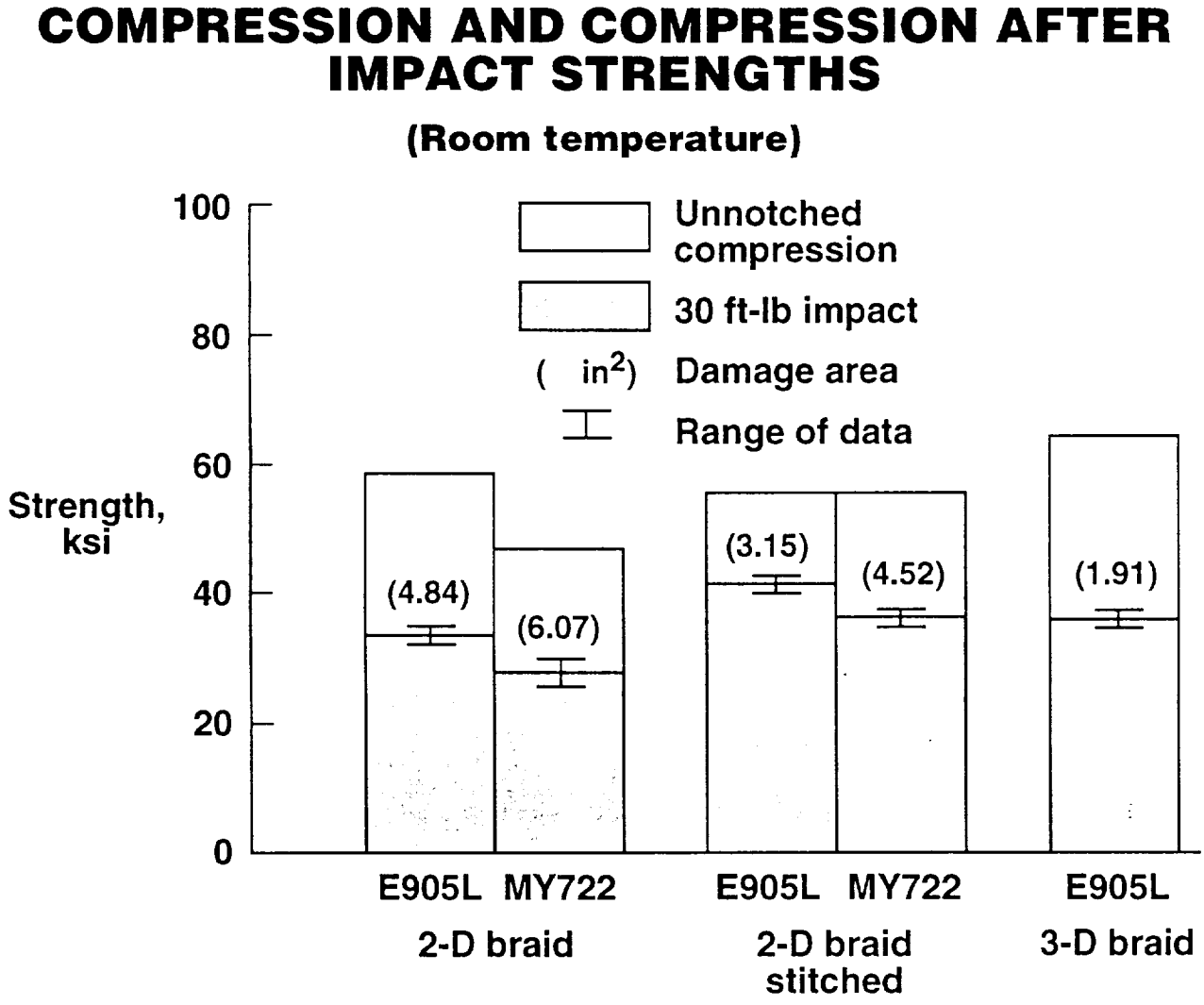

HOT/WET COMPRESSION AND COMPRESSION AFTER IMPACT STRENGTHS

The hot/wet CAI strengths of each braided composite are shown in figure 14. The unshaded bars are the hot/wet unnotched compression strengths from figure 11 and the shaded bars are the average hot/wet CAI strengths obtained from the impact specimens which were soaked in 160° F water for 45 days and then tested at 180° F, after the impact event. Only the 3-D/E905L composite had a repeat test under these conditions and the range is indicated on the figure. The stitched 2-D/E905L braid which exceeded 40 ksi CAI strength at room temperature (fig. 11) is shown to suffer the largest decrease in hot/wet CAI strength where a 25% decrease in the room temperature value is observed. The two stitched 2-D braids and the 3-D braid have about the same hot/wet CAI strengths, which are about 16% greater than the unstitched 2-D braided composites. Although only one hot/wet CAI test is reported for each 2-D and 2-D stitched braid composite, it is felt that these results are representative since small ranges in measured property values were obtained in the other hot/wet and notched compression test data previously discussed.

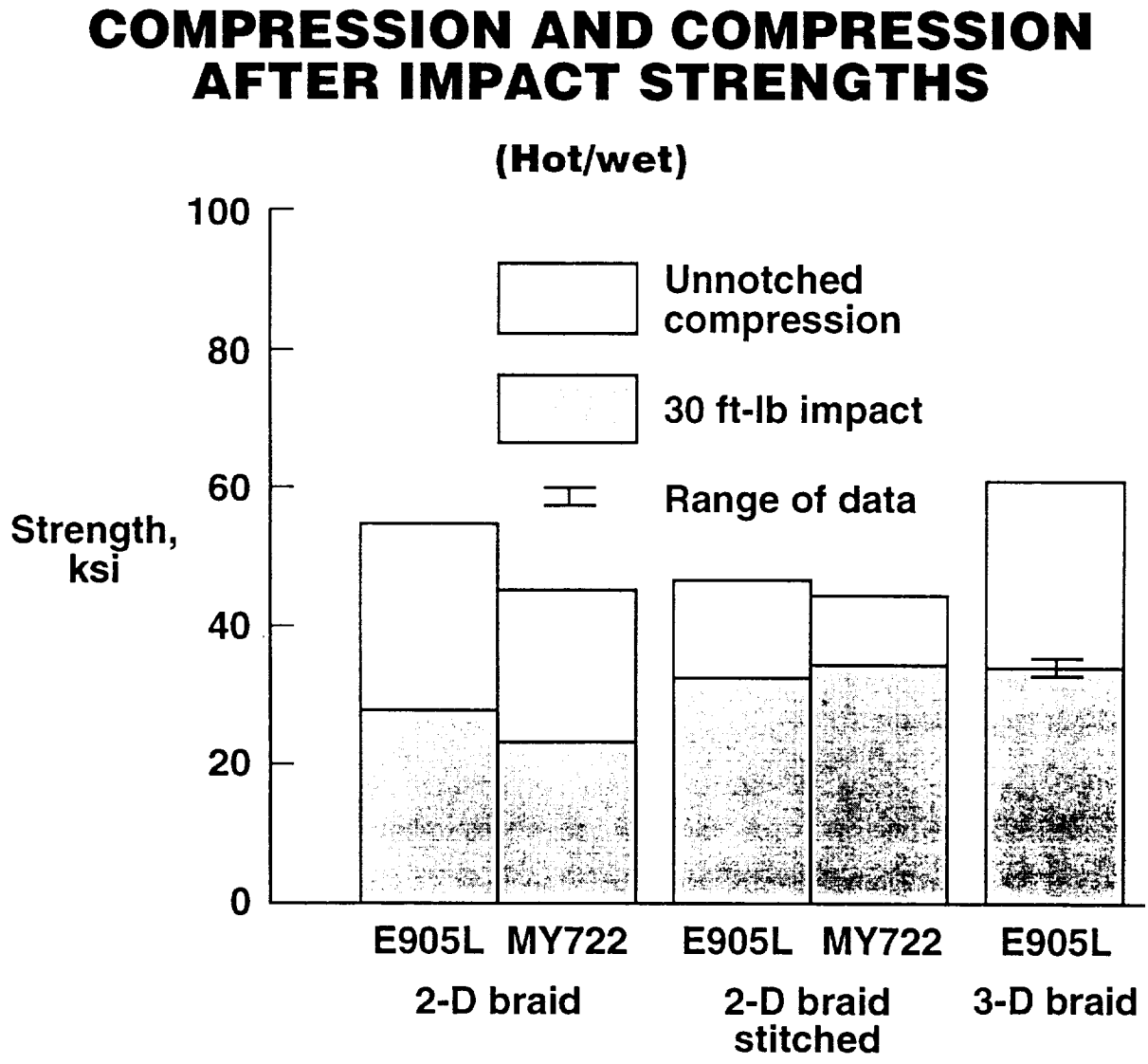

EFFECT OF HOLE SIZE ON COMPRESSIVE STRENGTHS

Figure 15 shows the effect of various hole diameters and specimen widths on the compressive strengths of the 3-D/E905L braid. The unnotched strengths were obtained from the 1.5-inch wide short block specimen data previously shown in figure 9. The data shown for the 0.25-in. diameter hole are also repeated from figure 9. In addition, two specimens having a 0.50-in. diameter hole and a specimen width of 3.0-inch, and two specimens having a 1.0-in. diameter hole and a specimen width of 5.0-inch were tested and the data is presented in the figure. Also shown on the figure is the CAI strength for this material (average damage area of 1.91-in.^{2} from figure 13). The data indicate a decrease in compression strength, compared to the unnotched strength, with increasing hole size.

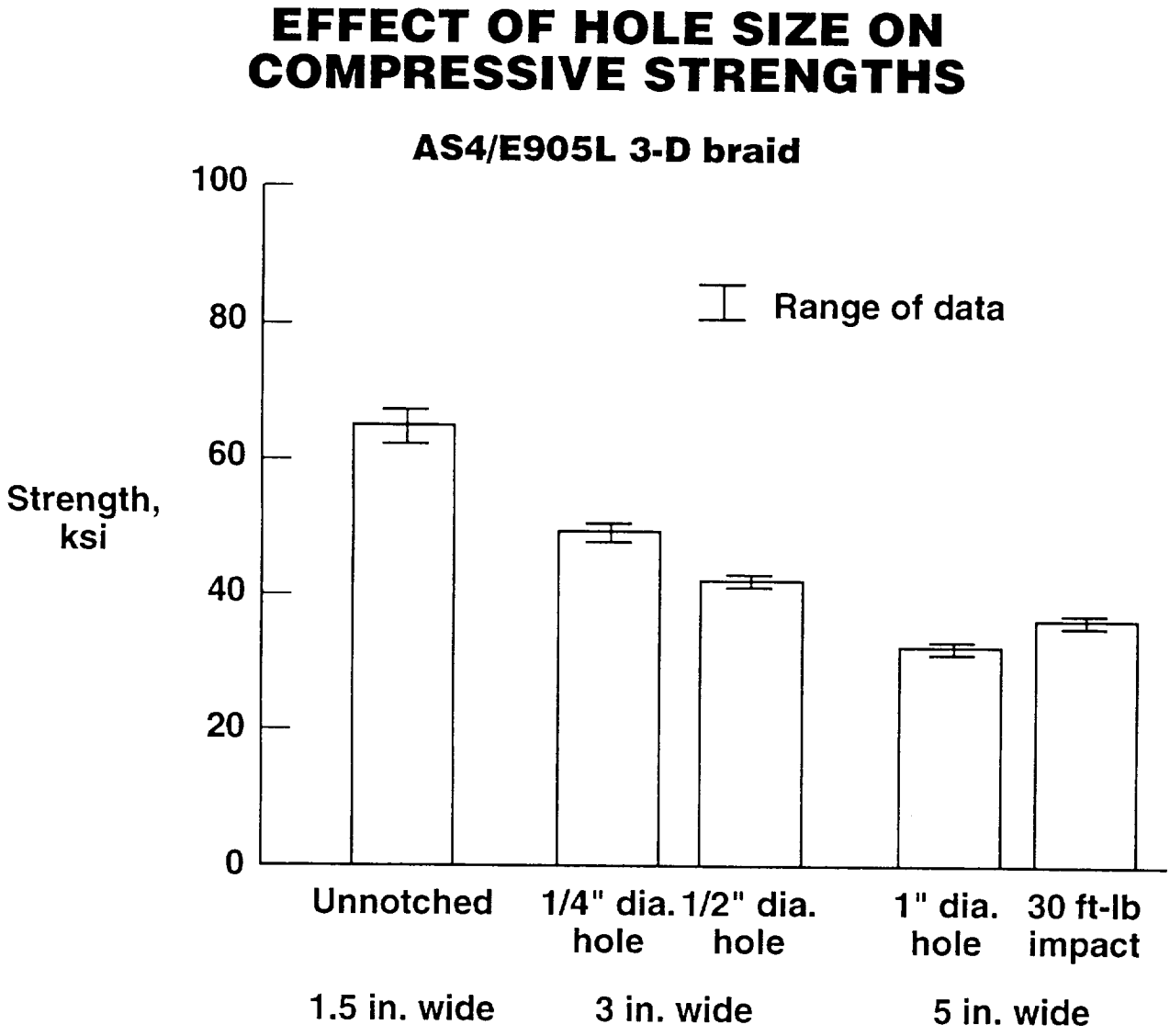

Figure 16 shows the 3-D fatigue test matrix and the number of specimens allotted for each of the test configurations previously described in figure 6. The baseline unnotched compression-compression and tension-tension fatigue tests have been completed and the results are discussed in subsequent figures. Drop weight impact at the first (30 ft-lb) of three energy levels has been performed and damage areas are being determined from C-scans prior to fatigue testing. All remaining fatigue test data will be reported at a future conference.

3-D BRAID FATIGUE TEST MATRIX

Unnotched tests:

10 specimens loaded in compression-compression fatigue

12 specimens loaded in tension-tension fatigue

Impact tests:

7 specimens at three impact levels loaded in compression

4 specimens at two impact levels loaded in tension

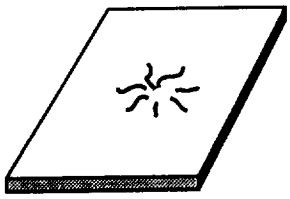

1/4 inch Open hole tests:

2 specimens static loaded in compression

16 specimens loaded in compression-compression fatigue

2 specimens static loaded in tension

10 specimens loaded in tension-compression fatigue

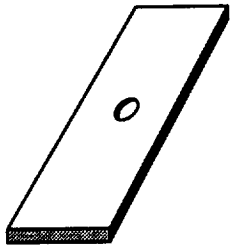

1/2 inch Open hole tests:

2 specimens static loaded in compression

4 specimens loaded in compression-compression fatigue

2 specimens static loaded in tension

4 specimens loaded in tension-compression fatigue

Maximum compressive stress is plotted against cycles to failure in figure 17. The value plotted at one cycle is the static failure stress from the room temperature short block compression test plotted in figure 9. A linear least squares regression fit to the data is also plotted. The linear regression fit to this data is the same as obtained in reference 6 for the same material tested with a constant cross-section area test section. The data shown in figure 17 indicates that the 3-D braids experienced a reduction in compression strength of about 44 % at 10^6 cycles. The 3-D braid material exhibits a wide range of fatigue lives for a fairly narrow range of cyclic stresses. This response is typical of that obtained in tape materials of similar constituents.

Airframe manufacturers typically design aircraft for a fatigue life of two lifetimes, where one cycle is equivalent to one takeoff and landing, and one lifetime is approximately 20 years or 60,000 hours of flight (see ref. 7). A design ultimate strain allowable of 0.004 has been suggested for tape laminates on the basis of damage tolerance. To evaluate the fatigue performance of the 3-D braided material, a region covering 1 to 2 lifetimes has been shaded and a dashed line placed at "limit condition" (2/3 times 0.004 strain level), based on the 3-D braided materials initial modulus given in figure 10. For wing bending on a typical transport aircraft, the strains will reach limit condition only a few times in a lifetime.

The compression fatigue response shows that the 3-D braid material, in the unnotched form, has more than adequate fatigue capability. The static strength of the notched 3-D braid was approximately 24 % less than the unnotched strength (fig. 9). Assuming that the slope of the S-N curve will be similar, the notched 3-D braid material may have marginal fatigue capability. The open-hole fatigue tests will help establish whether or not the 3-D braided material has adequate fatigue capability in compression.

COMPRESSION FATIGUE OF 3-D BRAIDS

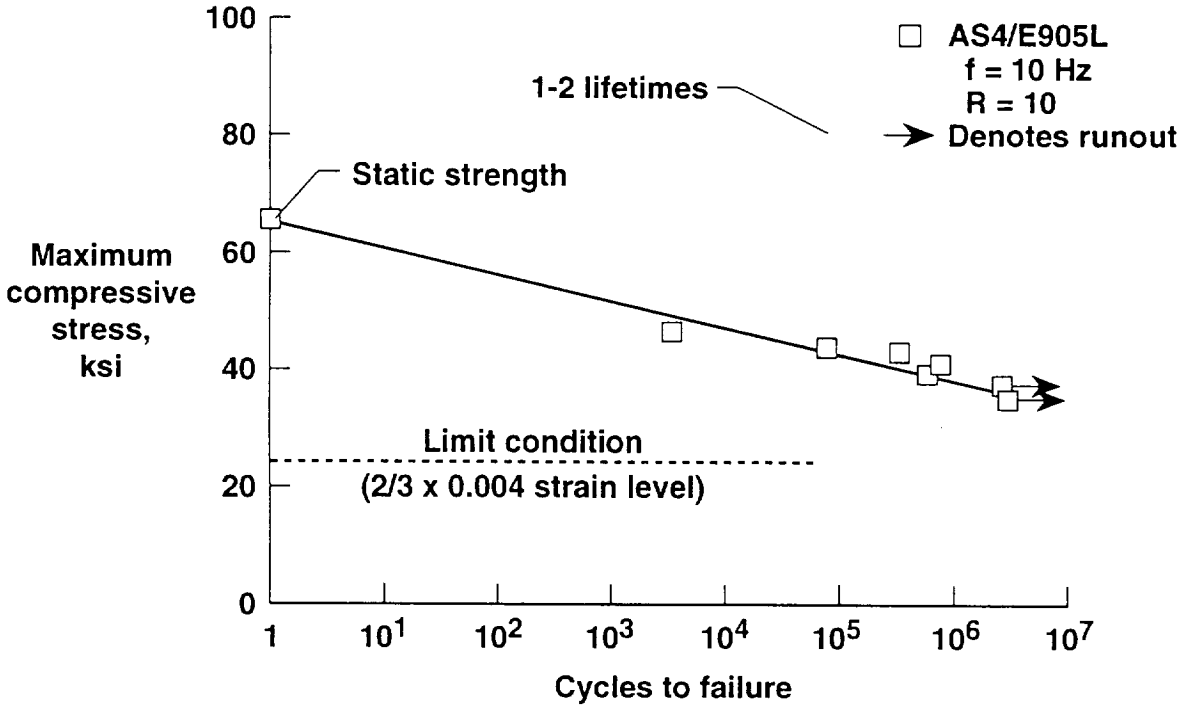

Figure 18 shows the maximum tensile stress plotted against cycles to failure for the 3-D braided material. The value shown for one cycle is the static failure stress from the room temperature tension test plotted in figure 7. A polynomial curve was fit to the data. The data shown in figure 18 indicates that the 3-D braids experienced a reduction in tensile strength with constant amplitude tension fatigue cycles of about 22 % at 10^6 cycles which is about one-half the loss experienced in compression fatigue at 10^6 cycles. For less than 10^5 cycles, the strength reduction was much less than that for compression fatigue data. Tensile strength is largely dependent upon the percentage of 0° fibers. The tension fatigue response of the 3-D braid material suggests that, although the off axis fibers may fail early in the life, the strength retains most of its initial unnotched strength.

Again, a region representing 1 to 2 lifetimes has been shaded and the design limit condition (2/3 times 0.004) is indicated on the figure by the dashed line. The unnotched tension fatigue response of the 3-D braid material is more than adequate. The notched static tension strength (fig. 7) is approximately 28 % less than the unnotched strength. Assuming the S-N responses to be similar, the notched fatigue response should also be more than adequate.

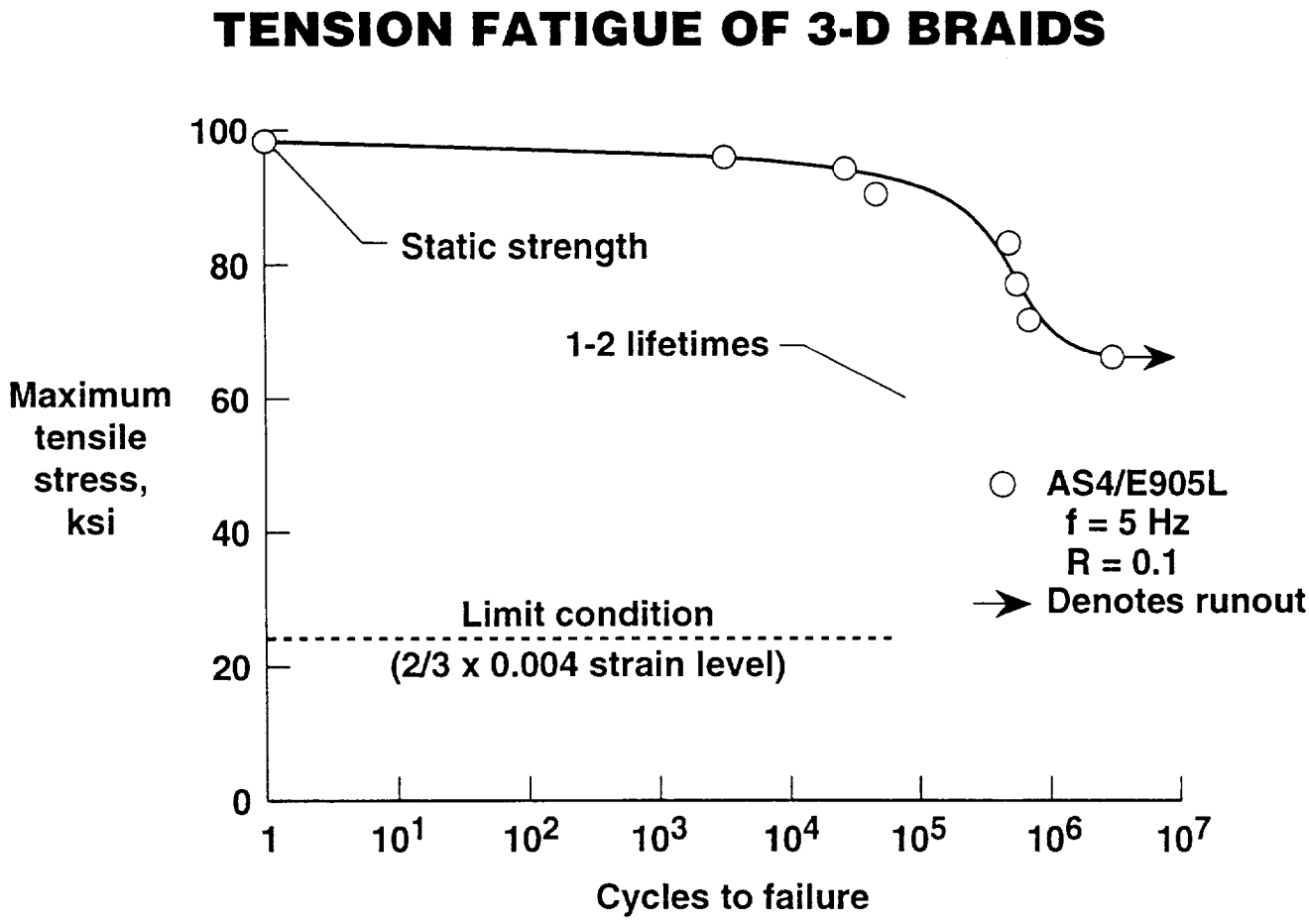

CONCLUDING REMARKS

Three different braided preform configurations, resin transfer molded with two different resin systems, have been evaluated to access their potential for applications to aircraft structures. The preforms evaluated include 2-D triaxial braid, 2-D triaxial braid with rows and columns of glass stitching, and 3-D through-the-thickness braid, all of which utilized AS4 12K graphite tows and the same [±30°/0°] braid architecture. The resin systems evaluated were British Petroleum E905L and Ciba Geigy MY722. Static mechanical tests were performed and include notched and unnotched tension, notched and unnotched compression, and compression after impact at room temperature and at 180° F after a 45 day water soak at 160° F. In addition to the static test performed, the baseline fatigue properties of the 3-D/E905L braided composite have been determined at room temperature. The results of this investigation support the following observations.

Static mechanical properties of the three braid architectures:

1. Unnotched tensile and compressive strengths varied among braided composites.

2. All notched tensile strengths were about equal.

3. Only the stitched 2-D/E905L composite exceeded a CAI strength of 40 ksi.

4. The 3-D braid has the best hot/wet notched compression and hot/wet CAI properties.

5. The 3-D braid appears to be showing the best overall combination of properties.

Fatigue results for 3-D/E905L braid:

1. Both unnotched tension and compression fatigue response are within current target values for fatigue life and strain levels for transport aircraft.

Future work will complete braided preform assessment.

REFERENCES

1. Palmer, Raymond J., Dow, Marvin B., and Smith, Donald L.: Development of Stitching Reinforcement for Transport Wing Panels, First NASA Advanced Composites Technology Conference, Seattle, WA, Oct. 29-Nov. 1, 1990. NASA CP-1304, Part 2, pp.621-646.

2. Dow, M.B., Smith, D.L., and Lubowinski, S.J.: An Evaluation of Stitching Concepts for Damage Tolerant Composites, Presented at Fiber-Tex 1988 Conference held in Greenville, South Carolina, September 13-15, 1988. NASA CP-3088, June 1989.

3. Dow, M. and Smith, D.: Damage-Tolerant Composite Materials Produced by Stitching Carbon Fabrics, International SAMPE Technical Conference Series, Volume 21, pp. 595-605.

4. Foye, R.L.: Finite Element Analysis of the Stiffness of Fabric Reinforced Composites, NASA CR 189597, February, 1992.

5. Masters, John E., Foye, Raymond L., Pastore, Christopher M., and Gowayed, Yasser A.: Mechanical Properties of Triaxially Braided Composites: Experimental and Analytical Results, NASA CR 189572, January, 1992.

6. Cano, Roberto J. and Furrow, Keith W.: Effects of Temperature and Humidity Cycling on the Strength of Textile Reinforced Carbon/Epoxy Composite Materials, Third Advanced Composites Technology Conference, NASA CP-3178.

7. Goranson, Ulf G. and Miller, Matthew: Aging Jet Transport Structural Evaluation Programs. Presented at the 15th Symposium of the International Committee on Aeronautical Fatigue (ICAF), Jerusalem, Israel, June 21-23, 1989.